ORIGINAL PAPER

The contribution of cationic conductances to the potential of rod photoreceptors

Andrea Moriondo · Giorgio Rispoli

Abstract The contribution of cationic conductances in shaping the rod photovoltage was studied in light adapted cells recorded under whole-cell voltage- or current-clamp conditions. Depolarising current steps (of size comparable to the light-regulated current) produced monotonic responses when the prepulse holding potential (V_h) was −40 mV (i.e. corresponding to the membrane potential in the dark). At $V_h = -60$ mV (simulating the steady-state response to an intense background of light) current injections <35 pA (mimicking a light decrement) produced instead an initial depolarisation that declined to a plateau, and voltage transiently overshot V_h at the stimulus offset. Current steps >40 pA produced a steady depolarisation to ≈ -16 mV at both V_h. The difference between the responses at the two V_h was primarily generated by the slow delayed-rectifier-like K$^+$ current (I_{Kx}), which therefore strongly affects both the photoresponse rising and falling phase. The steady voltage observed at both V_h in response to large current injections was instead generated by Ca-activated K$^+$ channels (I_{KCa}), as previously found.

Proceedings of the XIX Congress of the Italian Society of Pure and Applied Biophysics (SIBPA), Rome, September 2008.

A. Moriondo · G. Rispoli (✉)
Dipartimento di Biologia ed Evoluzione,
Sezione di Fisiologia e Biofisica,
National Institute of Neuroscience and Neuroscience Center,
Università di Ferrara, Via L. Borsari 46,
44100 Ferrara, Italy
e-mail: rsg@unife.it

Present Address:
A. Moriondo
DSBSC and Center for Neurosciences,
Università dell'Insubria,
Via J.H. Dunant 5, 21100 Varese, Italy

Both I_{Kx} and I_{KCa} oppose the cation influx, occurring at the light stimulus offset through the cGMP-gated channels and the voltage-activated Ca^{2+} channels (I_{Ca}). This avoids that the cation influx could erratically depolarise the rod past its normal resting value, thus allowing a reliable dim stimuli detection, without slowing down the photovoltage recovery kinetics. The latter kinetics was instead accelerated by the hyperpolarisation-activated, non-selective current (I_h) and I_{Ca}. Blockade of all K$^+$ currents with external TEA unmasked a I_{Ca}-dependent regenerative behaviour.

Abbreviations

C_m	Rod membrane capacitance
ChTx	Charybdotoxin
I_{Ca}	Voltage-activated Ca^{2+} current
I_{cG}	cGMP-gated Na$^+$ and Ca^{2+} current
I_{ClCa}	Ca-activated Cl$^-$ current
I_h	Hyperpolarisation-activated, non-selective cation current
I_{KCa}	Ca-activated K$^+$ current
I_{Kx}	Slow delayed-rectifier-like K$^+$ current
OS	Isolated rod outer segment
R_m	Rod membrane resistance
V_h	Holding potential

Introduction

Thirty years of comprehensive research has given a deep understanding of the light—activated enzymatic cascade which leads to the closure of the outer segment cGMP-gated

channels of vertebrate photoreceptors, producing photoreceptor hyperpolarisation (reviewed, for example, in: McNaughton 1990; Rispoli 1998; Moriondo and Rispoli 2003). The time course of the light-induced changes of the current entering the outer segment does not drive the inner segment voltage changes with the same time course, which ultimately modulates the rate of transmitter released at the synaptic terminal. The difference between the two time courses is produced by at least five kinds of voltage-sensitive channels located in the inner segment (reviewed in Barnes 1994): a nonselective cation current (I_h), a voltage-gated Ca^{2+} current (I_{Ca}), two Ca-activated currents permeable to Cl^- (I_{ClCa}) and to K^+ (I_{KCa}), and a voltage-gated, Ca-insensitive K^+ current (I_{Kx}; Attwell and Wilson 1980; Bader et al. 1982; Barnes and Hille 1989; Beech and Barnes 1989; Cia et al. 2005; Corey et al. 1984; Han et al. 2000; Hestrin 1987). Although these conductances have been extensively studied in both rods and cones, less attention has been devoted on how they shape the generator potential in response to light decrements. This is however an obvious key feature of the visual system in an enormous number of situations, from the swift detection of a predator's shadow to reading black letters on a white sheet of paper (Hurley 2002). We have previously described how I_{KCa} is able to clamp the photovoltage to its dark value (Moriondo et al. 2001). However, it is not clear yet how I_{KCa} and/or other voltage- and time- dependent cationic conductances affect the photoresponse kinetics and, in particular, the kinetics of the recovery of the generator potential to its dark level, once the light stimulus is terminated. This issue has been addressed in the following work by using rods mechanically isolated from *Ambystoma mexicanum* and recorded under whole-cell patch-clamp conditions.

Materials and methods

Animals and dissection

Ambystoma mexicanum larvae (20–25 cm length) were kept in deionised water supplemented with 1.55 g of marine salt per litre, in small tanks at room temperature (20–23°C), fed two-three times a week with earthworms and maintained in a natural light-dark cycle. Water change was performed once per week. The relative immobility of water and the constant ionic composition helped to preserve animals' health. Adequate care was taken to minimise pain and discomfort to animals, procedures and protocols were approved by the Institutional Animal Care Committee at the University of Ferrara, Ferrara, Italy, in accordance with the Health Research Extension Act.

The dissociation procedure has been slightly modified from the one already published (Moriondo et al. 2001).

Briefly, light-adapted and dark-adapted animals were anaesthetized with tricaine methanesulphonate 1 g/l, and subsequently decapitated and pithed. Both eyeballs were rapidly enucleated; the retina was dissected in standard external solution plus 1.5% foetal bovine serum (heat inactivated). The retina was triturated in 500 μl of standard external solution plus 1.5% foetal bovine serum with a P1000 pipette to obtain both intact photoreceptors and isolated rod outer segments (OS); the serum was found to improve the cell quality, leading to more stable whole-cell recordings. To record the photoresponses from OS, all the above manipulations were performed in the dark, using infrared illumination and an infrared viewer (Find-R-Scope, FJW Optical Systems, Palatine, IL, USA), on dark adapted animals (for ∼4 h).

Fifty microliter of cell suspension were plated onto 35 mm Petri dishes and let settle on ice for ≈30 min before filling the dish with 1.5 ml of standard extracellular solution and starting the experiment; OS were instead used immediately after the retina trituration.

Patch-clamp recordings

The patch-clamp set-up was made of an inverted microscope (IMT-2, Olympus) fitted with an Eppendorf PatchMan micromanipulator (Eppendorf, Hamburg, Germany). Rapid changes of the external solution were performed by moving by hand a multibarreled perfusion pipette in front of the recorded cell. The external solutions flowing in the perfusion pipette were gravity-fed (flow rate of 0.5–0.8 ml/min). Rod outer segments were illuminated with an ultrabright infrared LED (900 nm) and viewed on a TV monitor connected to a contrast enhancement camera (Till Photonics, Planegg, Germany). Light stimuli were delivered on dark adapted OS using pClamp voltage protocols: one of the two analogical outputs of the Digidata 1322A was connected to a calibrated voltage-to-current converter driving an ultrabright LED (555 nm) coupled to the binocular port of the microscope. The light emerging from LED passed through a neutral density filter (logarithmic attenuation factor: 2.0), a diffusion filter, a dicroic mirror (550 nm) housed in the exciter filter insertion slot and finally light was focused on the OS through a 60x objective. The LED was positioned so that the spot of light was focused and centered on the cell when the cell was viewed in sharp focus on the TV monitor. This set-up was enclosed in a Faraday's cage made with a copper's mesh, that was covered with a thick fully opaque cloth to carry on the experiments in the dark on the photoresponses from OS. The experiments on intact photoreceptors were instead carried out under room lights.

Electrical recordings were carried out at room temperature (20–22°C), using the patch-clamp recording technique

in the "whole-cell" configuration under visual control, employing an L/M-EPC7 patch-clamp amplifier (HEKA, Lambrecht, Germany). Current was filtered at 1.3 kHz by a low-pass Bessel filter (mod. LPBF-48DG, npi electronic GmbH, Tamm, Germany) and sampled at 10 KHz by a Digidata 1322A interface, connected to an AMD K6-2-400 mHz personal computer running Clampex 8.1 software (Axon Instruments, Foster City, CA, USA). Data were analysed offline by Clampfit 8.1; access resistance was compensated at 70%.

Solutions

Standard intracellular solution for recordings from intact cells contained (in mM): NaCl, 4; KCl, 105; EGTA free acid (ethylene glycol-bis-(β-aminoethyl ether)N,N,N',N',-tetraacetic acid), 5; MgCl$_2$, 2.5; HEPES free acid (N-[2-hydroxyethyl]piperazine-N'-[2ethanesulfonic acid]), 10; the intracellular solution for the OS recordings had the same composition but contained KCl, 95, adenosine 5'-triphosphate, dipotassium salt, 5, and guanosine 5'-triphosphate, sodium salt, 1. The pH and the osmolality of both solutions were adjusted to 7.2 with KOH and to 238 mOsm/Kg with D-glucose (usually 5 mM final concentration), respectively.

Standard extracellular solution contained: NaCl, 110; KCl, 2.5; CaCl$_2$, 1; MgCl$_2$, 1.6; HEPES free acid, 10; the pH and the osmolality were adjusted to 7.6 with NaOH and to 242 mOsm/Kg with D-glucose (usually 10 mM final concentration), respectively. Ba^{2+} and Cs$^+$ external solutions had the same formulation of the standard external solution, but 1 mM BaCl$_2$ substituted for CaCl$_2$ in the former, while the latter contained 100 mM NaCl and 10 mM CsCl. Extracellular solution for I_h recording contained: NaCl, 85; KCl, 2.5; TEACl, 30; CaCl$_2$, 1; MgCl$_2$, 1.6; CdCl$_2$, 0.2; HEPES, 10; pH 7.6, 242 mOsm/Kg.

Charybdotoxin (ChTx) was dissolved in standard external solution plus 0.01% bovine serum albumin to a final concentration of 100 nM. Tetrodotoxin was diluted to a final concentration of 2 μM from a 1 mM stock solution kept frozen. When used, CdCl$_2$ was added to the external solution to a final concentration of 200 μM from a 100 mM stock solution.

All chemicals were purchased from Sigma Aldrich (St. Louis, MO, USA) but ChTx and tetrodotoxin, purchased from Alomone Labs (Jerusalem, Israel), and foetal bovine serum and bovine serum albumin, purchased from GIBCO Life Technologies (Gaithersburg, MD, USA).

Stimulation with real flash responses

Responses to 5 ms flashes of light of increasing, sub-saturating intensity were recorded from isolated, dark-adapted OS recorded with the whole-cell voltage-clamp technique. To compensate for the different dark current amplitude (i.e. the current suppressed by a saturating step of light delivered just at the end of the response family) recorded from the outer segments, all flash responses were normalised to the average dark current (50 pA). The response family was then inverted and fed to Clampex as a stimulus protocol file.

Results are given as mean ± sem where appropriate.

Theory

Pure passive responses have been computed as follows:

$$
\begin{cases}
V(t) = V_h & \text{for } 0 \leq t < t_s \\
V(t) = V_h + R_m I_{stim}\left(1 - e^{\frac{-t+t_s}{R_m C_m}}\right) & \text{for } t_s \leq t < t_e \\
V(t) = V_h + R_m I_{stim} e^{\frac{-t+t_e}{R_m C_m}} & \text{for } t \geq t_e
\end{cases}
$$

where:

t	Time (ms)
t_s	Time to turn on the voltage pulse (ms)
t_e	Time to turn off the voltage pulse ($t_e - t_s =$ 500 ms)
V_h	Holding potential (mV)
R_m	Rod membrane resistance (GΩ)
C_m	Rod membrane capacitance (pF)
I_{stim}	Stimulus current (pA).

Results

### Voltage responses to current injections at $V_h = -40$ mV and $V_h = -60$ mV

To assess the role of the inner segment cationic conductances in shaping the recovery kinetics of the photoresponse, current-clamped rods were depolarised to various potentials using current injection steps of size similar to the light-regulated current (5–70 pA, lasting 500 ms; Fig. 1, *inset*). The steps were applied on top of a background current, whose amplitude was adjusted to have a steady membrane potential (V_h) of −40 mV (simulating the dark conditions) or −60 mV (simulating the steady-state response to a background of light). This strategy was therefore aimed at simulating also the photovoltage changes elicited by the reopening of the cGMP-gated channels following progressive reductions of intensity of a background of light. However, R_m (typically >1 GΩ) was higher compared to that of dark-adapted rods (typically ~370 MΩ), because the outer segment cGMP-gated channels are all closed in the present experiments, that were carried out under room lights.

At $V_h = -60$ mV, positive current injections generated an initial depolarisation which declined, often with damped

Fig. 1 Current-clamp voltage responses of a light-adapted rod starting from two different holding potentials (V_h).
a Responses to a series of increasing depolarising currents in 5 pA increments lasting 500 ms (*inset*) starting from an holding current (−9.3 pA in this cell) giving V_h = −60 mV.
b Same cell and stimulus protocol of **a**, but V_h = −40 mV (holding current: 35.8 pA).
c Voltage responses to a current injection of 25 pA (*upper panel*) and 70 pA (*lower panel*) superimposed to the pure passive responses computed from the measured R_m (1.2 GΩ) and C_m (26.1 pF; see Methods); V_h = −60 mV. **d** Same cell, protocol and simulations as **c**, but the current injections were 5 pA (*upper panel*) and 25 pA (*lower panel*); V_h = −40 mV
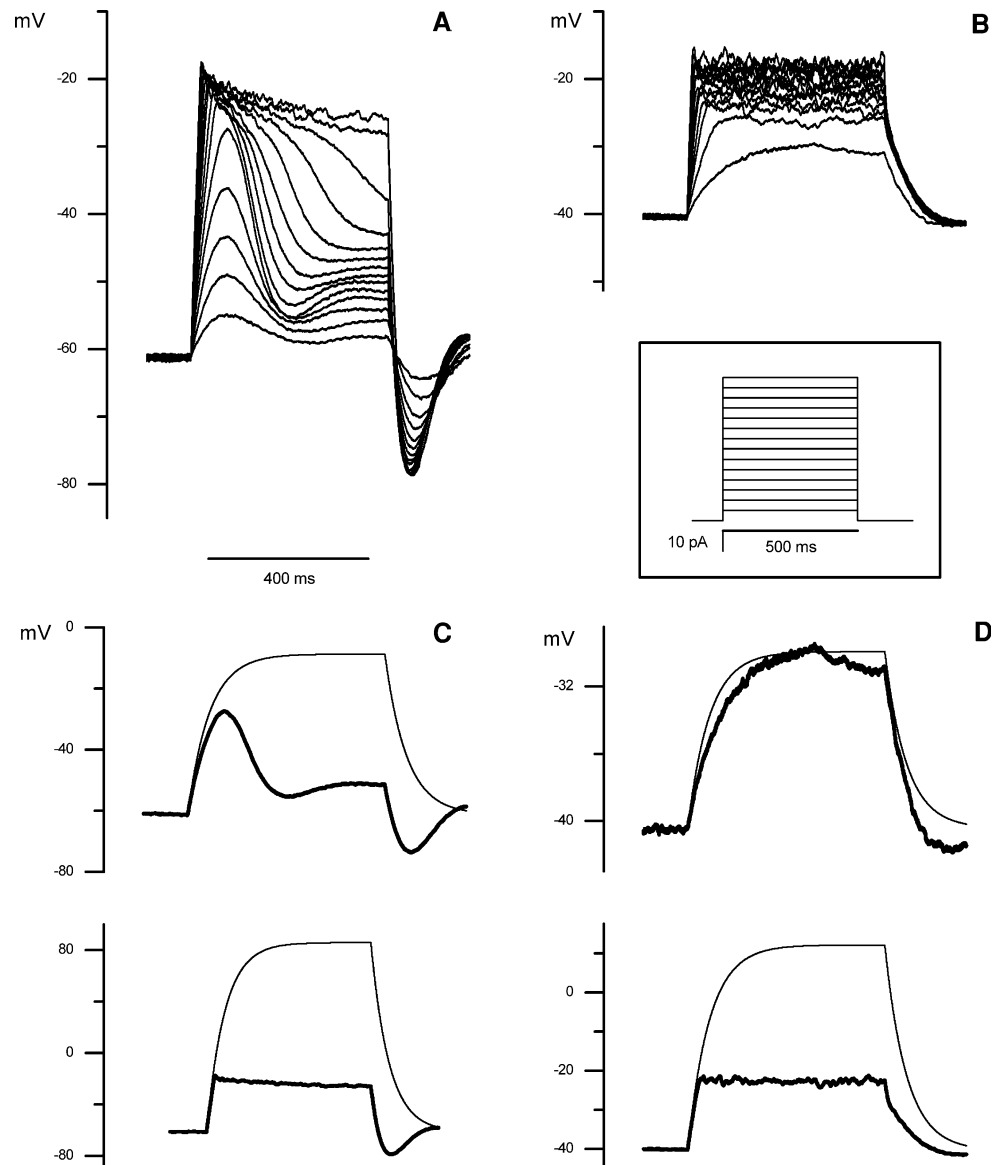
oscillations, to a plateau level. At the stimulus offset, the voltage transiently overshot the pre-stimulus level of −60 mV. By increasing the size of the injected current, the size of the voltage decline became smaller and its kinetics slower, but the peak amplitude of the overshoot at the stimulus offset was progressively enlarged. Moreover, the largest current stimuli (>40 pA) did not generate time-dependent voltage changes: the potential remained instead substantially stable to a saturating level of −15.7 ± 2.7 mV (maximum amplitude for a 70 pA current injection, n = 6; Fig. 1a). If the holding current was adjusted to give V_h = −40 mV (corresponding to dark conditions), the voltage responses were dramatically different in respect to the ones obtained at V_h = −60 mV. Indeed, neither the voltage decline nor the overshoot were observed but the responses were just monotonic. However, as the injected current was made larger, the "voltage saturation effect" of Fig. 1a was

still present (average amplitude for a 70 pA current injection: −16.2 ± 1.1 mV, n = 7; Fig. 1b). The above results show that some voltage- and/or time- dependent conductances are recruited during the current injections, and this would therefore strongly affect the recovery phase of the light response. The effectiveness of these conductances is shown in Fig. 1c, d, where the pure passive responses, computed from the measured R_m and C_m (see Methods), are compared to the actual voltage responses for two current injections delivered at V_h = −60 mV (Fig. 1c; 25 pA, *upper panel*; 70 pA, *lower panel*) and at V_h = −40 mV (Fig. 1d, 5 pA, *upper panel*; 25 pA, *lower panel*). It is clear that only the 5 pA current injection at V_h = −40 mV can be (barely) fitted. Therefore, at least one outward delayed current must be activated during the stimulus, resulting in voltage response compression. Voltage-clamp experiments indicated that this was the case: a delayed current was

indeed progressively activated following a depolarisation from $V_h = -60$ mV (Fig. 2a); this current was therefore already active at $V_h = -40$ mV (Fig. 2b).

For both V_h, another noisy outward component appeared to be abruptly activated for depolarisations more positive than -30 mV. Moreover, when hyperpolarising from -60 mV, a progressively activating inward current was recorded, which should necessarily comprise the now deactivating above mentioned current already active at -40 mV. It is clear that it is necessary to pharmacologically dissect the contribution of the diverse cationic components in order to understand the ionic bases of the above voltage responses.

I_{KCa}, I_{Ca}, and I_h contribution to voltage responses

A possible candidate acting as an outward delayed current is I_{KCa} (Moriondo et al. 2001): therefore, the experiments
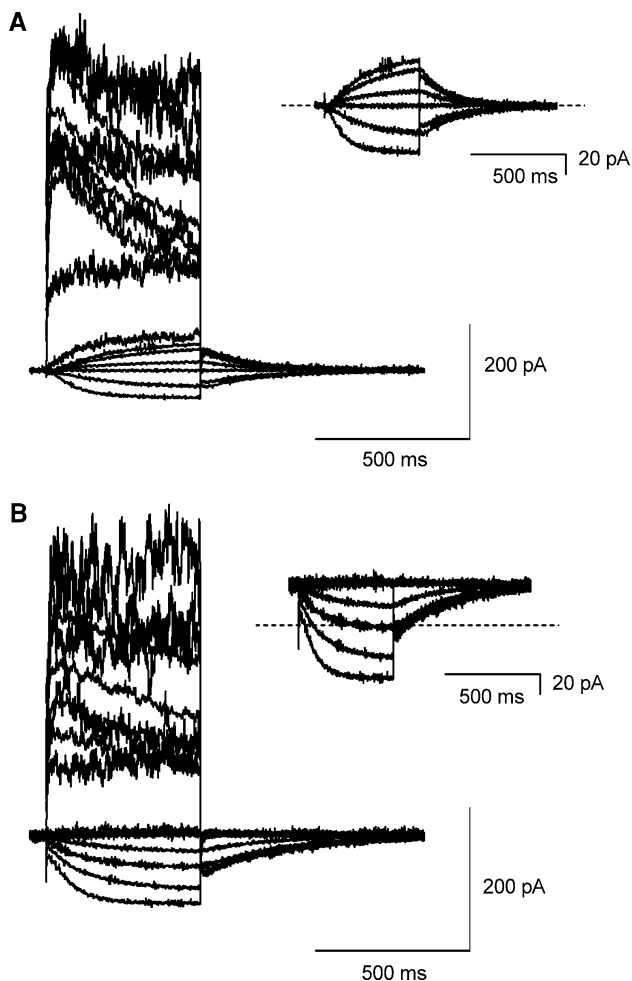
Fig. 2 Voltage-clamp current responses of a rod starting from two different holding potentials. **a** Responses to a series of 500 ms voltage pulses from -80 to 70 mV in 10 mV increments starting from $V_h = -60$ mV; the responses to voltage pulses from -80 to -30 mV are enlarged in the *inset*. **b** Same as **a**, but $V_h = -40$ mV. *Dotted line* indicate zero current level

of Fig. 1 were repeated during extracellular perfusion with 200 μM Cd^{2+} (which blocks I_{Ca}, and, indirectly, I_{KCa}) or 100 nM ChTx (a scorpion venom known to selectively block I_{KCa}). The voltage decline during the current injection and the overshoot at the stimulus offset observed at $V_h = -60$ mV were unaffected by Cd^{2+} application, indicating that neither I_{KCa} nor I_{Ca} produced these features in the voltage responses (Fig. 3).

Moreover, the voltage saturation effect shown in Fig. 1 was lost in the presence of Cd^{2+} or ChTx, irrespective of the initial V_h (Figs. 3, 4), showing that this effect was produced by I_{KCa} activation. Given the time-dependent waveform of the voltage response in current-clamp experiments, the current-to-voltage plots (I–V) were computed by averaging the points at about the voltage peak just following the current injection onset (where $dV(t)/dt \approx 0$; Figs. 3c, 4d, e, *empty symbols*) and by averaging the last 20 ms of the response (where again $dV(t)/dt \approx 0$; Figs. 3c, 4d, e, *filled symbols*). Clearly, the voltage increased upon increasing the size of the injected current in the presence of Cd^{2+} (Figs. 3c, 4d, *squares*) or ChTx (Fig. 4e, *squares*) instead of being clamped at about -16 mV as in control (70 pA current stimulus; Figs. 3c, 4d, e, *circles*; Figs. 3a, 4a). In detail, a 70 pA injection gave a maximal depolarisation of -0.8 ± 2.0 mV (Fig. 3b, c, $n = 6$) at $V_h = -60$ mV in the presence of Cd^{2+} and 31.4 ± 5.5 mV (in Cd^{2+}; Fig. 4b, d, $n = 7$) and 24.5 ± 7.1 mV (in ChTx; Fig. 4c, e, $n = 7$) at $V_h = -40$ mV. This shows again the effectiveness of I_{KCa} at clamping the photovoltage to values close to the dark potential (Moriondo et al. 2001).

In conclusion, neither I_{KCa} nor I_{Ca} generated the voltage decline and the overshoot of the current-clamp responses at $V_h = -60$ mV (Fig. 1a). I_h did not either generate the latter response features, since it is not expected to be active for any potential more positive than -60 mV (Fig. 6g).

Indeed, I_h blockade by the external application of 10 mM Cs^+ (or 10 mM $Cs^+ + 200$ μM Cd^{2+}; Fig. 5) did not affect the waveform of the photovoltage in response to depolarising current injections.

I_{Kx} contribution to voltage responses

The last candidate explaining the peculiar features of the response at $V_h = -60$ mV is the non-inactivating, slow delayed-rectifier-like K^+ current (I_{Kx}; Attwell and Wilson 1980; Barnes and Hille 1989). The simplest approach to study I_{Kx} is to subtract from the control traces the ones where I_{Kx} is fully blocked. Unfortunately, no selective blockers of I_{Kx} are yet available: a non-specific one is Ba^{2+} (Beech and Barnes 1989; Wollmuth 1994; Fig. 6), because concentrations as high as 1 mM of this ion (replacing 1 mM external Ca^{2+}) were necessary to shift the channel voltage half-activation (estimated from the plot of the
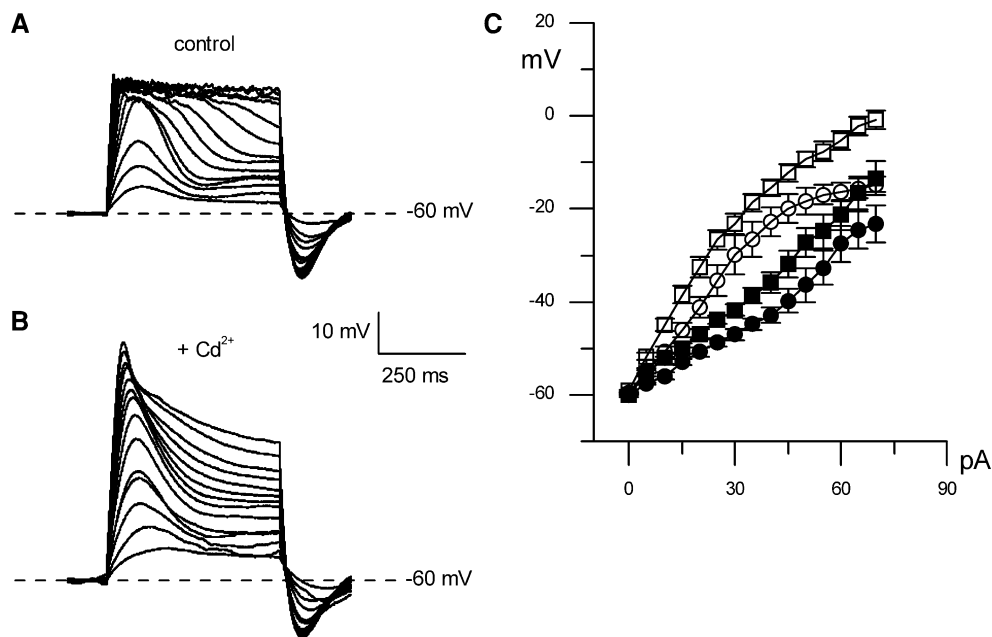
Fig. 3 Effect of I_{Ca} and I_{KCa} blockade on the current-clamp voltage responses at $V_h = -60$ mV. **a** Control recording. **b** Application of 200 μM Cd^{2+}. **c** Current-to-voltage plots (*I–V*), computed by averaging the points just following the current injection onset (where

$dV(t)/dt \approx 0$; *empty symbols*) and by averaging the last 20 ms of the response (where again $dV(t)/dt \approx 0$; *filled symbols*) in control (*circles*) and after the application of 200 μM Cd^{2+} (*squares*)

tail-current amplitude vs. test voltage; Fig. 6h) of about 17.2 mV (i.e. from -50.5 ± 0.5 mV in control to -33.3 ± 0.7 mV in 1 mM Ba^{2+}, $n = 4$). To isolate the effect of Ba^{2+} on I_{Kx}, the Ca^{2+} channels (and the Ca-activated conductances as well), were blocked by the external application of Cd^{2+}. Moreover, Ba^{2+} ions screen the cell surface membrane charges less well than Ca^{2+}: therefore, the voltage activation curve of any voltage-dependent channel would be subjected to a negative shift once the external Ca^{2+} is substituted for Ba^{2+} (for example, this shift is about -6 mV for Na^+ channels; Hille et al. 1975). Therefore, the shift in the voltage half-activation of I_{Kx} would result larger than 17 mV once corrected for the surface charge screening effect. In addition to the effect on I_{Kx}, Ba^{2+} application seems to block the currents elicited by the hyperpolarisation to -70 and -80 mV (compare the *insets* of Fig. 6e, f). This effect could be explained by assuming that the latter traces are generated by I_{Kx} deactivation (i.e. I_{Kx} is thought to be still active at -60 mV), their size being reduced in Fig. 6f due to the Ba-induced shift of their voltage activation curve. However, this is not the case, because these two traces were still present when I_{Kx} was fully blocked by 30 mM TEA (Fig. 6g), but they were cancelled by 10 mM Cs^+ application (Fig. 8c, d). Therefore, they were generated by I_h activation, and their apparent block in the presence of 1 mM external Ba^{2+} is very likely due to the shift of I_h voltage activation curve

towards negative values, caused by the aforementioned Ba^{2+} screening effect.

I_{Kx} could be isolated by blocking all the other known current sources present in the rod inner segment by using 200 μM Cd^{2+} and 10 mM Cs^+. Assuming that I_{Kx} is not sensitive to the latter ions (as also indicated in Frings et al. 1998), the panels c and f of Fig. 5 illustrate the voltage changes produced by the isolated I_{Kx} in response to current injection steps. The size of these voltage changes indicated that I_{Kx} is a robust current, that was therefore studied under voltage-clamp conditions while perfusing the rod with Cd^{2+} and Cs^+ (Fig. 7).

As expected, the waveform of the currents recorded in response to depolarisations in Cd^{2+} (Fig. 7a, b) were almost identical to the ones recorded in $Cd^{2+} + Cs^+$ (Fig. 7c, d), irrespective of the initial V_h. I_{Kx} gate is very slow for voltages between -60 and -30 mV (Fig. 7, *insets*), as indicated by the single-exponential fittings to its activation and deactivation waveforms. Indeed, a depolarisation to -30 mV, starting from a V_h of -60 or -40 mV, gave an average activation and deactivation time constant of 280 ± 31 and 115 ± 14 ms ($n = 8$), respectively. These time constants were even larger for smaller depolarisations: a 10 mV step from V_h of -60 or -50 mV gave an average activation and deactivation time constant of 471 ± 95 and 344 ± 31 ms ($n = 8$), respectively. This slow gating explains well the voltage decline of the responses during

Fig. 4 Effect of selective block of I_{Ca} and I_{KCa} on the current-clamp voltage responses at $V_h = -40$ mV. **a** Control recording. **b** Application of 200 μM Cd^{2+}. **c** Application of 100 nM ChTx. **d** Current-to-voltage plots (I–V), computed as in Fig. 3, in control (*circles*) and after application of 200 μM Cd^{2+} (*squares*). **e** Same as **d**, but the I–V indicated by the *squares* refers to 100 nM ChTx. Cd^{2+} and ChTx were applied on two distinct cell populations instead of on the same population in two following applications: this strategy excluded possible interactions between the effects of the two drugs, due to incomplete wash. The I–V resulting from the application of Cd^{2+} (**d**) and ChTx (**e**) are plotted against their own control (although both controls were nearly identical)
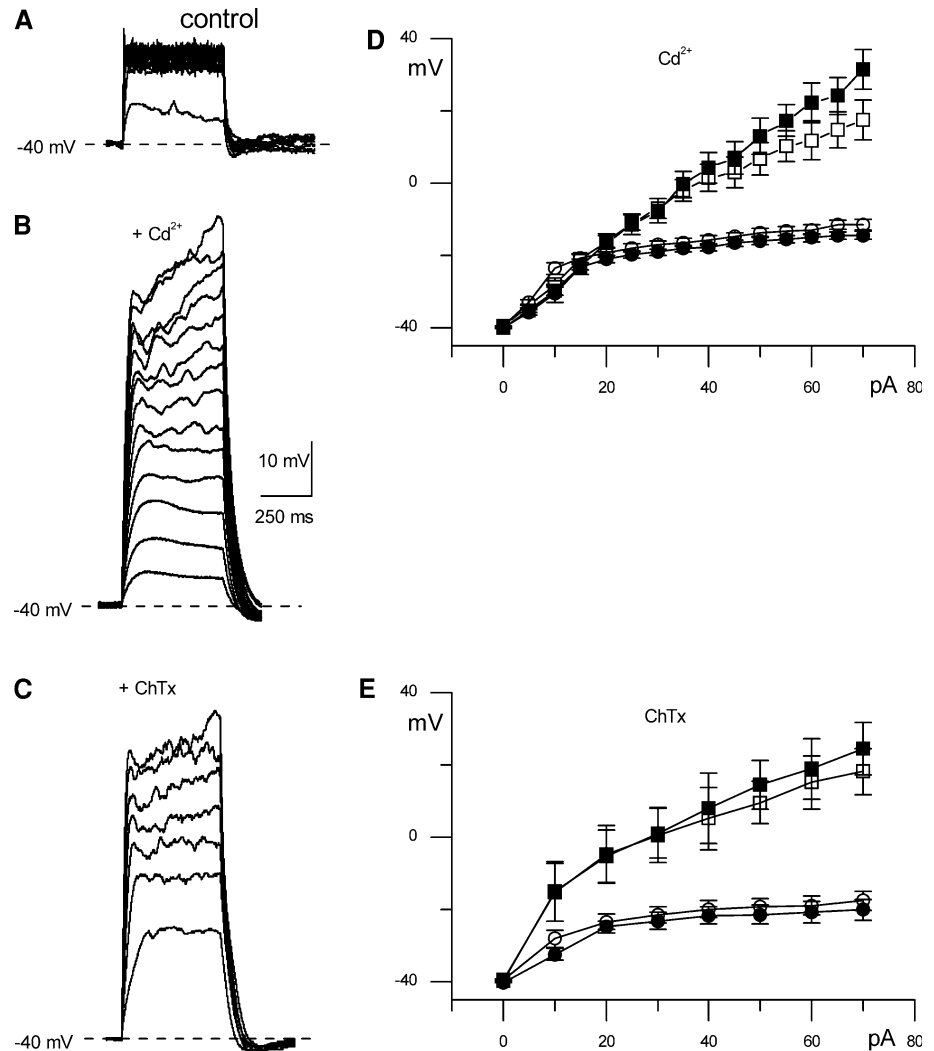
the current injection and the overshoot at the stimulus offset (Fig. 1a). Remarkably, for voltages more positive than -10 mV the current decayed with time, after an initial peak, in a voltage independent manner (Fig. 7a–d).

In conclusion, I_{Kx} is the major current contribution shaping the overall photoresponse: since current injections employed so far are step-wise, it would be important to see how I_{Kx} affects the response to a current stimulation with the same time-dependent waveform of the real photoresponse, delivered in the "dark" (i.e. at -40 mV) and on a "background of light" (i.e. at -60 mV). To this aim, current-clamped rods were challenged with stimulation protocols derived from real photocurrent families recorded from OSs of dark-adapted rods (see Methods for details, Fig. 8a), and extracellularly perfused with Cd^{2+}-Cs^+, to isolate I_{Kx} as the only current not blocked. The activation of I_{Kx} by setting V_h to -40 mV, produced a transient overshoot of the pre-stimulus voltage level in the recovery phase of the flash response. This overshoot was absent

when V_h was set to -60 mV (below the activation threshold of I_{Kx}).

I_{Ca} accelerates the photoresponse rising phase and generates spikes

In the presence of Cd^{2+}, R_m increases since two conductances are blocked: therefore, Cd^{2+} is expected to slow down the kinetics of the voltage change produced by a given current injection, while it is expected to boost the response amplitude. Indeed, the response rise time in Cd-treated cells became significantly larger in respect to the control (Fig. 9a) for current injections ≥ 10 pA ($p < 0.01$, ANOVA, $n = 5$; Fig. 9b). While increasing the current injection amplitude, the rise time steadily increased to a plateau level of 41.2 ± 2.9 ms in Cd^{2+} and of 13.1 ± 0.5 ms in control. However, the voltage amplitude in response to a given current stimulus in the presence of Cd^{2+} was smaller with respect to the control (Fig. 9a).
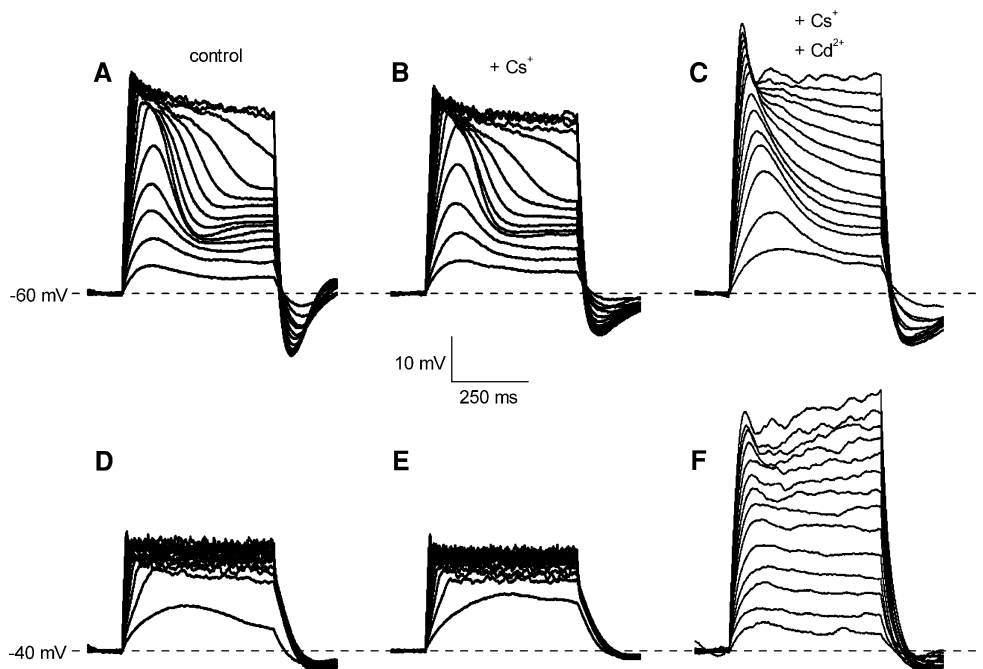
Fig. 5 Effect of I_h, I_{Ca} and I_{KCa} blockade on the current-clamp voltage responses at $V_h = -60$ mV (**a**, **b** and **c**) and $V_h = -40$ mV (**d**, **e** and **f**). Stimulus protocol as in Fig. 1 (*inset*). **a**, **d** Control. **b**, **e** Application of 10 mM Cs^+. **c**, **f** Application of 10 mM Cs^+ +200 µM Cd^{2+}

The full block of I_{Kx} (and the block of all the K^+ currents as well, but the I_h) was obtained with external TEA application (30 mM) which, on the other hand, produced an auto-regenerative voltage response to depolarising current injections. Spikes were consistently recorded in all cells when $R_m > 1$ GΩ, and they were clearly evidenced at $V_h = -60$ mV (Fig. 10a), where progressively larger current injections produced progressively faster depolarisations to an average steady state amplitude of 17.7 ± 2.3 mV ($n = 11$; $R_m \approx 1.3 \pm 0.1$ GΩ). Even if the injected current was turned off, this depolarised level was often maintained for a longer duration in tighter cells (rods reported in Fig. 10a, b are an example; mean duration: 12.7 ± 1.9 s, $n = 6$; range: 2.4–64 s). This indicates that the eventual recovery to V_h, once the stimulating current was turned off, was basically controlled by the leakage. This recovery occurred at progressively earlier times when recording from the same cell for several minutes, suggesting the involvement of I_{Ca} in spike generation. Consistently with this view, the spike threshold amplitude (-28.1 ± 0.6 mV, $n = 5$) was close to the I_{Ca} one. The former was assessed as the voltage amplitude where the first derivative of the membrane potential departed from a constant value in response to current ramps of same maximal amplitude (100 pA) and of duration varying from 70 to 7,000 ms (data not shown; threshold was not affected by the ramp steepness). Moreover, spikes were unaffected by 2 µM tetrodotoxin, but they were abolished by 200 µM Cd^{2+} and the voltage responses were almost identical to the

ones generated by a circuit formed by the parallel between R_m and C_m (Fig. 10b), as described in Theory.

Discussion

Contribution of Na^+, Ca^{2+} and K^+ fluxes to the rod photoresponse

In the dark, there is a steady flow of Na^+ into the photoreceptor carried by the current through the cGMP-gated channels (I_{cG}), a steady influx of Ca^{2+} via the I_{cG} and I_{Ca}, and a steady outflow of K^+ via the I_{Kx} and the I_{KCa}, while $I_h \approx 0$. The resulting membrane permeability to Na^+ (P_{Na}), K^+ (P_K), and Ca^{2+} (P_{Ca}) generates a membrane potential V_m that is ≈ -40 mV in the dark, that can be roughly accounted for by the equation:

$$V_m = \frac{RT}{2F} \cdot \ln\left(\frac{P_{Na}[Na]_o + P_K[K]_o + 4P_{Ca}[Ca]_o}{P_{Na}[Na]_i + P_K[K]_i + 4P_{Ca}[Ca]_i}\right)$$

that has been computed using the Goldman-Hodgkin-Katz formalism in the reasonable assumption that:

$$P_{Na} \approx P_K \quad [Na]_i \approx [K]_o \quad [Na]_o \approx [K]_i$$

and where R, T and F have the usual meaning. During light stimulation, the inflow of Na^+ and Ca^{2+} via the I_{cG} is reduced, and the following hyperpolarisation decreases I_{Kx}, I_{Ca}, and, in turn, I_{KCa} due to the resulting $[Ca^{2+}]_i$ fall. Therefore, the rising phase of the light-induced

Fig. 6 I_{Kx} and I_h waveforms recorded in current-clamp (**a**, **b** and **c**; stimulus protocol as in Fig. 1) and in voltage-clamp (**d**, **e**, **f** $V_h = -60$ mV, stimulus protocol as in Fig. 2a, b; **g** $V_h = -30$ mV, stimulus protocol consisting of 500 ms voltage pulses steps from -40 to -120 mV in 10 mV increments) and effect of Ba^{2+} on their voltage sensitivity. **a**, **d** Controls. **b**, **c**, **e**, **f** Application of 200 μM Cd^{2+}. **c**, **f** 1 mM Ca^{2+} was substituted with 1 mM external Ba^{2+}. *Scale bar* of **d**, **e**, **f** is indicated in between **e** and **f**, but *vertical scale bar* of **d** is indicated on its right. Responses to voltage pulses from -80 to -30 mV of **e** and **f** are enlarged in the corresponding *inset* on the right of each panel; the two *insets* have the same *scale bar*. **g** isolation of I_h with 30 mM TEA (see Methods); the fast transients at the onset and the offset of the voltage pulses are capacitative artefacts. **h** Plot of the normalised peak tail current amplitude from **e** (*circles*) and **f** (*squares*) vs. test potential ($n = 4$)
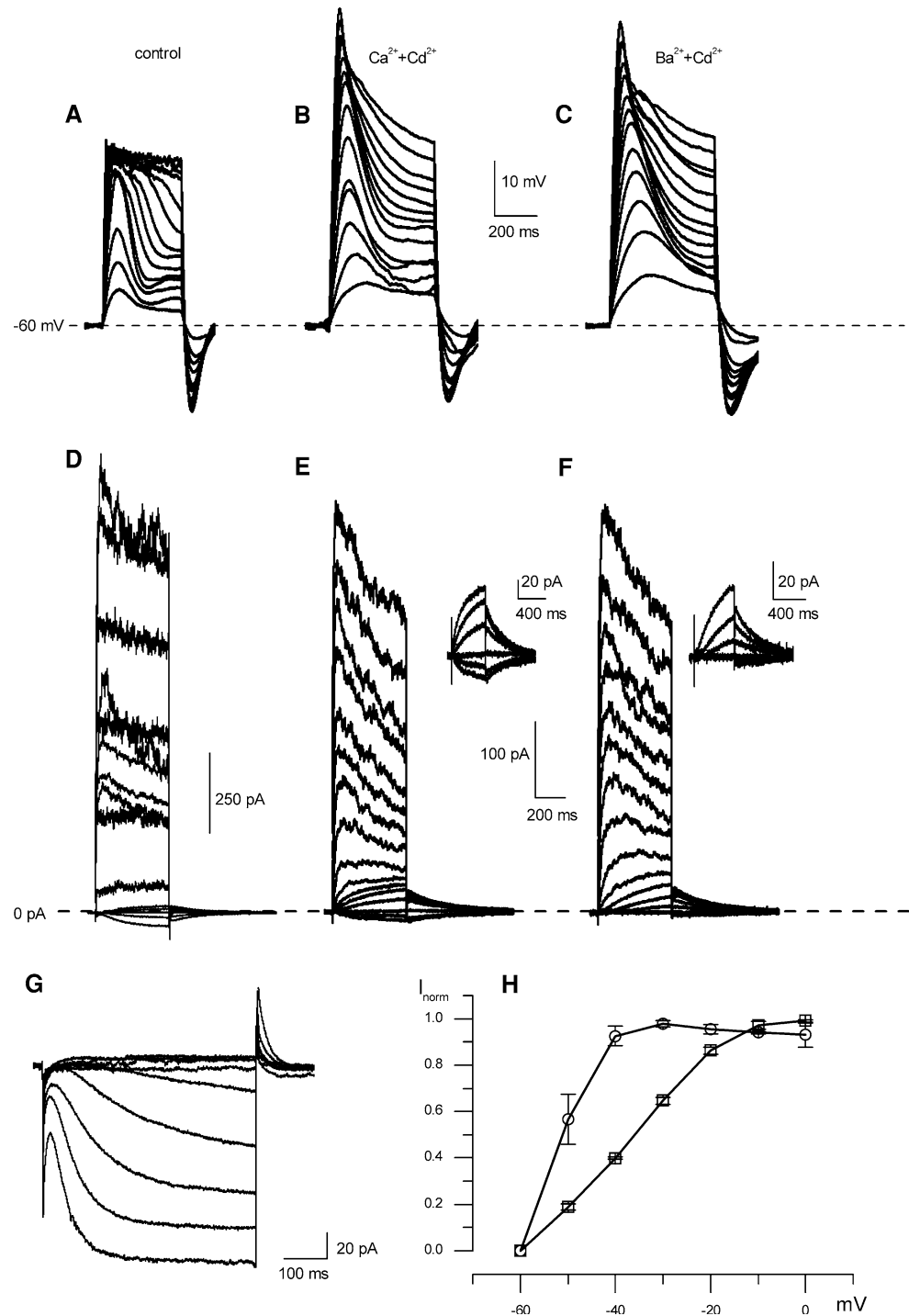
hyperpolarisation is expected to be accelerated by the decreased inflow of Ca^{2+} (as shown in Fig. 9) and slowed-down by the decreased outflow of K^+. On the other hand, I_{Kx} (and, to a lesser extent, I_{KCa}) has a very slow gating (Fig. 7) with respect to I_{cG} and I_{Ca}: as a result, the outflow of K^+ is still sustained in the early phase of the photoresponse, actually leading to an acceleration of its rising phase (Barnes and Hille 1989; Fig. 7). Moreover, large

hyperpolarisations (i.e. in the presence of strong light stimuli) activate I_h and produce a net cation inward current that hinders the hyperpolarisation kinetics. Since I_h, I_{Kx} and I_{KCa} gate with 100–200 ms relaxation times (at room temperature), they cause the voltage response to light to fade during the first 100–200 ms, producing therefore sensory adaptation. This adaptation sums up to the one occurring at the level of the enzymatic cascade that

Fig. 7 Voltage-clamp recording of $I_{Kx} + I_h$ (**a, b**) and I_{Kx} (**c, d**) at $V_h = -60$ mV (**a, b**) and $V_h = -40$ mV (**b, d**). **a, b**: Application of 200 μM Cd^{2+}. **c, d** Application of 10 mM Cs^+ 200 μM Cd^{2+}. The responses to voltage pulses from −80 to −30 mV are enlarged in the four insets for each V_h and ion application; *dotted line* indicates the zero current level. All responses are normalised to the same amplitude but the four insets, having all the same *scale bar*. Stimulus protocol of **a** and **c** (and relative insets) as in Fig. 2a, b; stimulus protocol of **b** and **d** (and relative insets) as in Fig. 2c
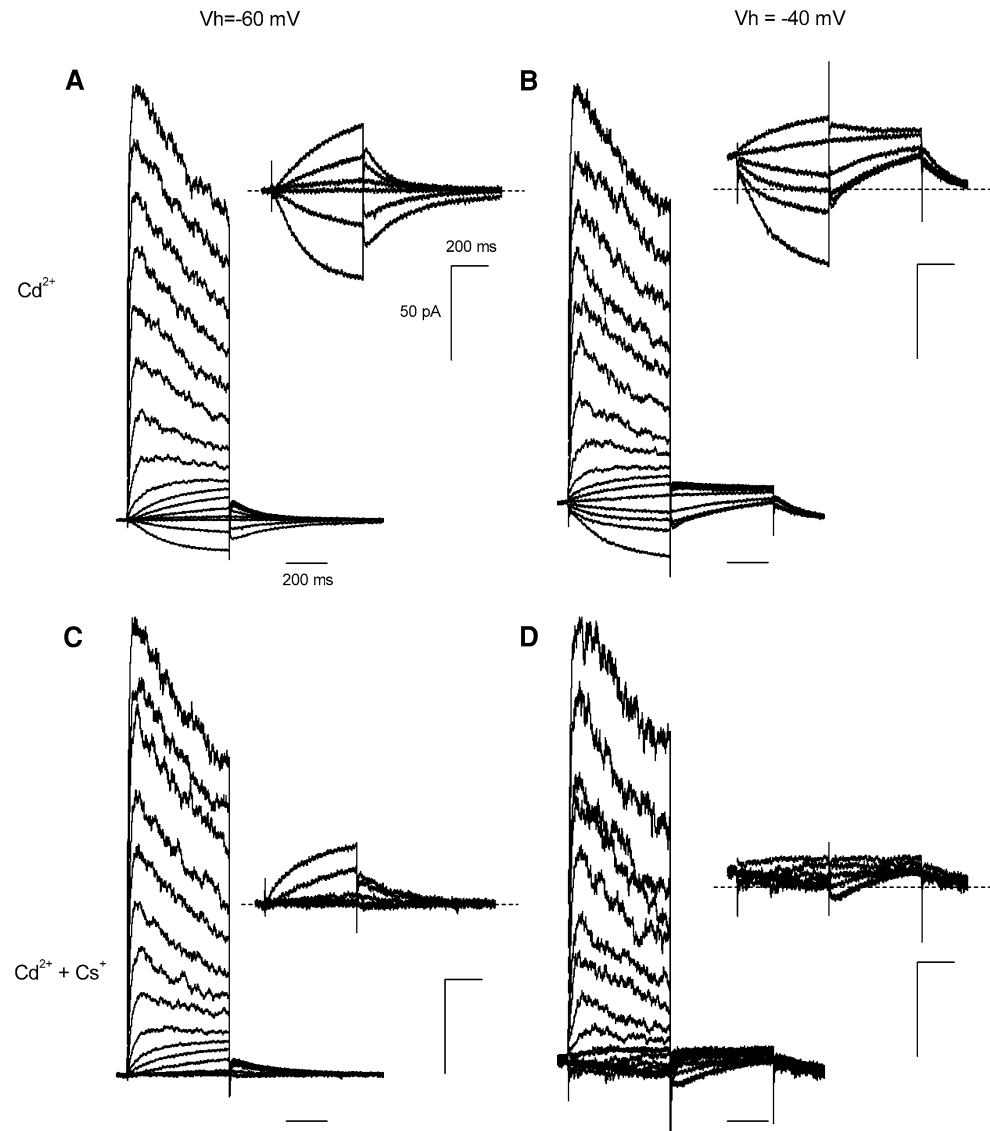
progressively re-opens a fraction of the cGMP-gated channels in the presence of prolonged illuminations, leading to a further amplitude compression of the voltage response. Once the light stimulus is terminated and the I_{cG} is progressively restored to its dark level, the following depolarisation is accelerated by I_h, which has a fast deactivation kinetics (Fig. 6g). I_{Ca} activation also contributes to this acceleration, especially in the range of current injections above 10 pA, corresponding to the changes produced by the I_{cG} reactivation when moderate to saturating light intensities are turned off (Fig. 9b). This is also evident in Fig. 9a, where the response amplitude to a given current injection (*thin* trace) is decreased when I_{Ca} is blocked (*thick* trace). Given the voltage sensitivity of I_h and I_{Ca}, this acceleration is particularly large once intense light stimuli are turned off, providing a mechanism that quickly de-saturates the photoreceptor. I_{Ca} activation and I_h

deactivation produce therefore high pass filtering of the light response. Both I_{Kx} and I_{KCa} avoid that cation influx, occurring at the light stimulus offset via the I_{cG} and the I_{Ca}, could erratically depolarise the rod past its normal resting value. The slow gating of I_{Kx} allows that the above "dark voltage stabilisation" occurs without slowing down the early phase of the photoresponse recovery kinetics. The latter is also accelerated by I_{Kx} when the light stimuli are delivered in the dark with respect to the ones delivered on a background of light, where the responses are anyway greatly accelerated as a results of the feedback regulation of the enzymatic cascade (reviewed in Moriondo and Rispoli 2003). This allows the photoreceptor to integrate light for relatively long time to maximise the sensitivity, without slowing down the recovery kinetics of the response. On the other hand, response amplitude is little affected by the voltage (Fig. 8) when I_{Kx} is the solely

Fig. 8 Photoresponse families recorded in current clamp at $V_h = -40$ and -60 mV in Cd^{2+}-Cs^+ extracellular solution, in response to current stimuli shown in the upper panel. The stimulus protocol consisted in whole-cell current responses to 5 ms flashes of intensities: 12.5, 25, 51.2 and 101.6 Rh*/flash recorded from a dark-adapted OS; dark current amplitude of all responses was normalised to 50 pA. *Lower panel*: superimposition of the photoresponses obtained with the largest current stimulus at V_h −40 mV (*thick trace*) or −60 mV (*thin trace*). *Dotted trace* represents the scaled and inverted current stimulus
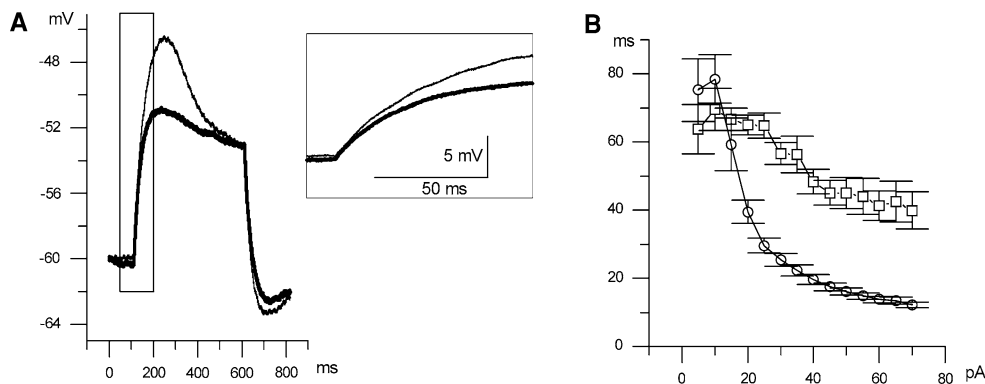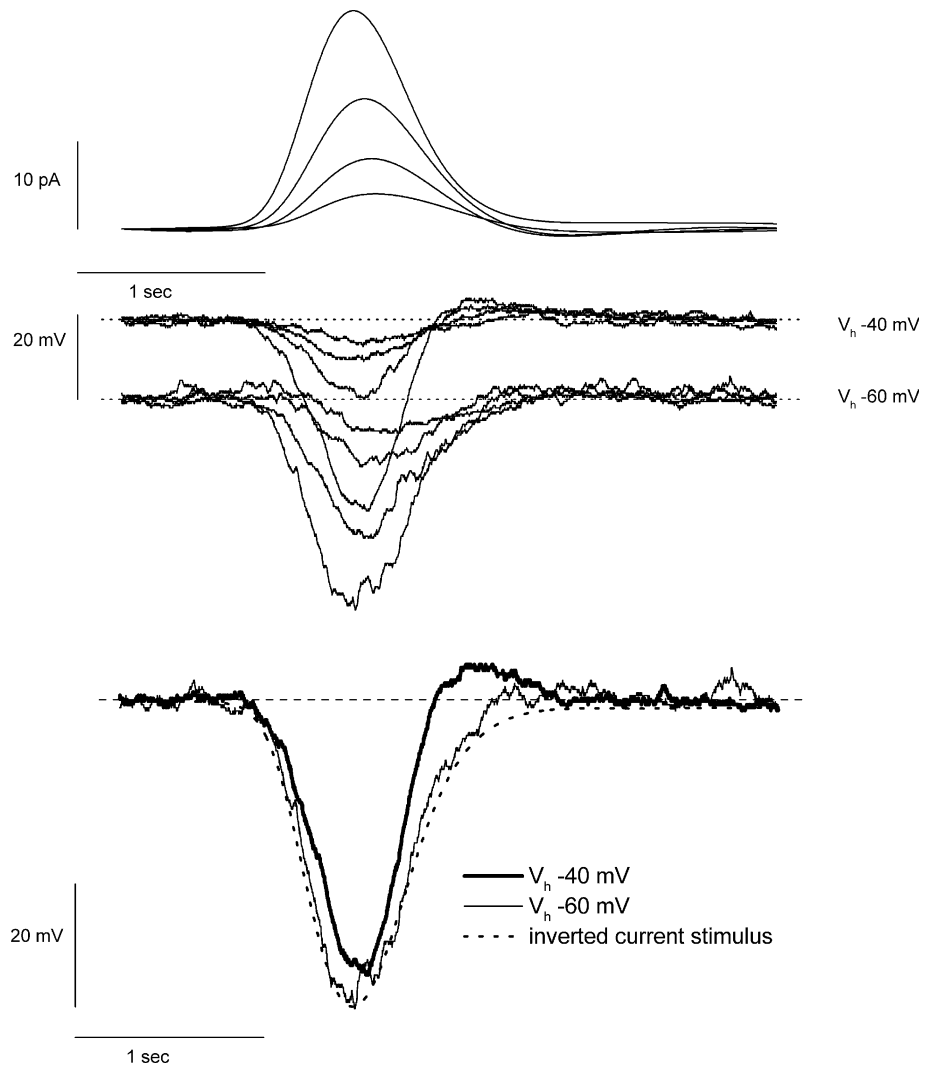

Fig. 9 Effect of I_{Ca} blockade on the rise time of the current-clamp voltage responses at $V_h = -60$ mV. **a** Voltage response to a 15 pA current injection in control (*thin trace*) and after application of 100 μM Cd^{2+} (*thick trace*); the rising phase of both responses is enlarged in the *inset*. **b** 10–90% rise time of the voltage response for current injections from 5 to 70 pA in 5 pA increments in control (*circles*) and after application of 100 μM Cd^{2+} (*squares*). The rise time of the responses to 60, 65 and 70 pA current injections were averaged in both conditions

active current: the latter does not therefore contribute to the photoreceptor desensitization (i.e. the reduction of response amplitude when it is superimposed on a background of

light). I_{Kx} affects rather the response kinetics, which nevertheless plays a key role in the rod performances, given that second-order retinal neurons primarily sense changes

Fig. 10 Effect of I_{Kx}, I_{KCa} and I_{Ca} blockade on the current-clamp voltage responses at $V_h = -60$ mV. **a** Voltage responses to current injections from 65 to 85 pA in 5 pA increments lasting 500 ms of a rod with $R_m \approx 600$ MΩ perfused with 30 mM TEA. **b** Response to repetitive 40 pA current injections in a rod perfused with 30 mM TEA (*thin trace*) and with 30 mM TEA + 200 μM Cd²⁺ (*thick trace*); R_m was ≈2.6 GΩ, ≈405 MΩ, ≈920 MΩ, and ≈1.1 GΩ just before, and after 1, 21, and 41 s from the first current injection, respectively. All recordings were obtained in 200 μM tetrodotoxin
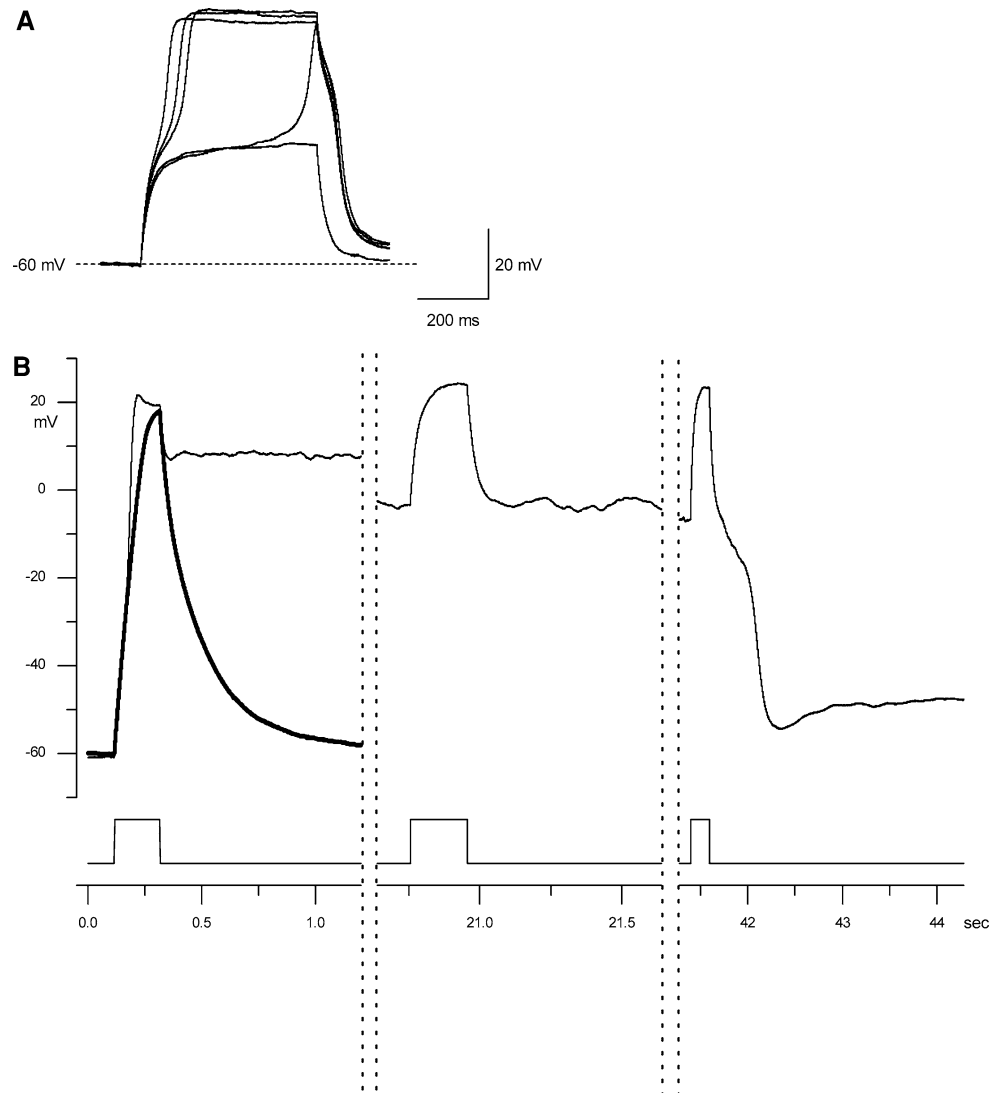
in the presynaptic response rather than its steady state level. In conclusion, I_{Kx} and I_{KCa} give a key contribution to the exquisite sensitivity of the rod visual system (which is able to signal the ∼1.5 mV hyperpolarisation following the absorption of a single photon), by minimising also the low-frequency voltage fluctuations that may occur in the dark (Moriondo and Rispoli 2003).

The similarity between the responses of Fig. 5c and f with the ones of Fig. 1a and b, respectively (apart the voltage saturation effect due to I_{KCa} activation), shows that the differences between the response families at $V_h = -40$ mV and at $V_h = -60$ mV are mainly due to I_{Kx} gating. In particular, I_{Kx} and I_{Ca} are inactive at $V_h = -60$ mV: positive current injections (simulating the off of the light stimulus) rapidly activate I_{Ca}, which accelerates the rising phase of the voltage response. Current injection also turns on I_{Kx} (Fig. 8d), whose slow activation accounts for the voltage decline of the responses of Fig. 1a, especially for amplitudes between 5 and 30 pA, i.e. just in the range of the current

changes produced by dim to sub-saturating light intensities. Larger current injections abruptly activate I_{KCa} (with a fast kinetics; Moriondo et al. 2001) if the following depolarisation is larger than 30 mV: this activation produces the voltage saturation effect described above. At $V_h = -40$ mV, I_{Kx} is already active: progressively increasing positive current injections activate I_{Kx} and I_{Ca} with progressively faster kinetics (Fig. 8b) leading to monotonic voltage responses, as shown in all responses of Fig. 1b and for current injections above 50 pA in Fig. 1a. Finally, further current injections abruptly activate I_{KCa}, producing again the aforementioned voltage saturation effect.

Spikes

The lack of stability of the dark potential when I_{KCa} and I_{Kx} are blocked is indicated by the generation of spikes observed in rods perfused with Ba²⁺ or Sr²⁺ (Beech and Barnes 1989; Brown and Flaming 1978) and by the large

depolarisations observed in dark-adapted rods perfused with ChTx (Moriondo et al. 2001) or when blocking all the K^+ currents with TEA (Fig. 10). The action potentials recorded from the low vertebrate rods are not generated by voltage-gated Na^+ channels, as in human photoreceptors (Kawai et al. 2001), but rather by I_{Ca} activation, as previously found in toads (Fain et al. 1980), turtles (Gerschenfeld et al. 1980), lizards (Maricq and Korenbrot 1988; reviewed in Owen 1987), and primates (Schnapf et al. 1990). Curiously, no Na^+ current was found in porcine photoreceptors: this difference may arise from the cell preparation, since human rods were recorded in retinal slices (Kawai et al. 2001) whereas porcine photoreceptors (Cia et al. 2005) and salamander rods (present study) were recorded from dissociated cells, that could have lost some cell parts where the voltage-gated Na^+ channels could be entirely segregated. However, the porcine photoreceptor images reported in the Cia et al. (2005) study showed remarkably intact cells, and we also fail to record Na^+ spikes even in the most intact rods, retaining the synaptic pedicle. Therefore, the presence of Na^+ spikes in mammalian photoreceptors could be restrained to human retina only.

The eventual recovery to V_h once the injected current is turned off (Fig. 10) is basically governed by the leak. This explains why this recovery took minutes to occur in the tighter cells (Fig. 10b). It can be therefore concluded that K^+ conductances can stabilise the voltage to the dark level, avoiding spike priming which would therefore occur when these conductances are blocked (by TEA, ChTx, Ba^{2+}, or Sr^{2+}).

The spike generation is a Ca-dependent process, since it is blocked by the presence of extracellular Cd^{2+}, but it can not be excluded that I_{ClCa} channels (Maricq and Korenbrot 1988; Barnes and Deschênes 1992) could be implicated in this phenomenon. Indeed, the average sustained depolarisation voltage in the recordings of Fig. 10 is -1.82 ± 0.75 mV ($n = 6$), in good agreement with the Cl^- equilibrium potential of -1.10 mV, calculated by the Nernst equation from the Cl^- concentrations used in the intracellular and extracellular solutions, therefore it is possible that I_{ClCa} could be involved in spike generation. Nevertheless, the peak membrane potential recorded at spike early times is about 18 mV (Fig. 10a, see "Results"), which is more positive than the Cl^- equilibrium potential: therefore, I_{Ca} plays a major role in shaping the spike rising phase.

Nature of I_{Kx}

In all voltage-clamp recordings of rod I_{Kx} presented here, there was a marked current decline for depolarisations larger than -10 mV (Figs. 6e, f, 8; Wollmuth 1994). No

sign of such decline has been observed for voltages up to 50 mV in mammalian rods (Cia et al. 2005). I_{Kx} was remarkably similar to the current recorded from two splice variants of an *ether-à-go-go* channel cloned from bovine retina (named bEAG1 and bEAG2; Frings et al. 1998), transiently expressed in HEK293 cells, as regard ion selectivity, blockage, voltage activation, Ba^{2+} inhibition and Cs^+/Cd^{2+} sensitivity. About 80% of the voltage-clamp recordings obtained by Frings et al. (1998) from bEAG1 and bEAG2 (see their Fig. 3) did not show any current decline for any voltage, as found in mammalian rod I_{Kx}; the remaining recordings (20%) did instead show a pronounced current decline for voltages larger than $+30$ mV, as found in salamander rod I_{Kx}. This gives the attractive perspective that I_{Kx} of vertebrate photoreceptors are coded by the same *ether-à-go-go* gene, and the differences in the electrophysiological features arise from some post-transcriptional modifications.

References

Attwell D, Wilson M (1980) Behaviour of the rod network in the tiger salamander retina mediated by membrane properties of individual rods. J Physiol 309:287–315

Bader CR, Bertrand D, Schwartz EA (1982) Voltage-activated and calcium-activated currents studied in solitary rod inner segments from the salamander retina. J Physiol 331:253–284

Barnes S (1994) After transduction: response shaping and control of transmission by ion channels of the photoreceptor inner segments. Neurosci 58:447–459. doi:10.1016/0306-4522(94)90072-8

Barnes S, Deschênes MC (1992) Contribution of Ca and Ca-activated Cl channels to regenerative depolarization and membrane bistability of cone photoreceptors. Neurophysiol 68:745–755

Barnes S, Hille B (1989) Ionic channels of the inner segment of tiger salamander cone photoreceptors. J Gen Physiol 94:719–743. doi:10.1085/jgp.94.4.719

Beech DJ, Barnes S (1989) Characterization of a voltage-gated K^+ channel that accelerates the rod response to dim light. Neuron 3:573–581. doi:10.1016/0896-6273(89)90267-5

Brown DT, Flaming DG (1978) Opposing effects of calcium and barium in vertebrate rod photoreceptors. Proc Natl Acad Sci USA 75:1587–1590. doi:10.1073/pnas.75.3.1587

Cia D, Bordais A, Varela C, Forster V et al (2005) Voltage-gated channels and calcium homeostasis in mammalian rod photoreceptors. J Neurophysiol 93:1468–1475. doi:10.1152/jn.00874.2004

Corey DP, Dubinsky JM, Schwartz EA (1984) The calcium current in inner segments of rods from the salamander (*Ambystoma tigrinum*) retina. J Physiol 354:557–575

Fain GL, Gerschenfeld HM, Quandt FN (1980) Calcium spikes in toad rods. J Physiol 303:495–513

Frings S, Brüll N, Dzeja C et al (1998) Characterization of ether-à-go-go channels present in photoreceptors reveals similarity to I_{Kx}, a K^+ current in rod inner segments. J Gen Physiol 111:583–599. doi:10.1085/jgp.111.4.583

Gerschenfeld HM, Piccolino M, Neyton J (1980) Feed-back modulation of cone synapses by L-horizontal cells of turtle retina. J Exp Biol 89:177–192

Han Y, Jacoby RA, Wu SM (2000) Morphological and electrophysiological properties of dissociated primate retinal cells. Brain Res 875:175–186. doi:10.1016/S0006-8993(00)02614-7

Hestrin S (1987) The properties and function of inward rectification in rod photoreceptors of the tiger salamander. J Physiol 390:319–333

Hille B, Woodhull AM, Shapiro BI (1975) Negative surface charge near sodium channels of nerve: divalent ions, monovalent ions, and pH. Philos Trans R Soc Lond B Biol Sci 270:301–318. doi:10.1098/rstb.1975.0011

Hurley JB (2002) Shedding light on adaptation. J Gen Physiol 119:125–128. doi:10.1085/jgp.119.2.125

Kawai F, Horiguchi M, Suzuki H, Miyachi E (2001) Na(+) action potentials in human photoreceptors. Neuron 30:451–458. doi:10.1016/S0896-6273(01)00299-9

Maricq AV, Korenbrot JI (1988) Calcium and calcium-dependent chloride currents generate action potentials in solitary cone photoreceptors. Neuron 1:503–515. doi:10.1016/0896-6273(88)90181-X

McNaughton PA (1990) Light response of vertebrate photoreceptors. Physiol Rev 70:847–883

Moriondo A, Rispoli G (2003) A step-by-step model of phototransduction cascade shows that Ca^{2+} regulation of guanylate cyclase accounts only for short-term changes of photoresponse. Photochem Photobiol Sci 2:1292–1298. doi:10.1039/b303871h

Moriondo A, Pelucchi B, Rispoli G (2001) Calcium-activated potassium current clamps the dark potential of vertebrate rods. Eur J NeuroSci 14:19–26. doi:10.1046/j.0953-816x.2001.01605.x

Owen WG (1987) Ionic conductances in rod photoreceptors. Annu Rev Physiol 49:743–764. doi:10.1146/annurev.ph.49.030187.003523

Rispoli G (1998) Calcium regulation of phototransduction in vertebrate rod outer segments. J Photochem Photobiol B 44:1–20. doi:10.1016/S1011-1344(98)00083-9

Schnapf JL, Nunn BJ, Meister M et al (1990) Visual transduction in cones of the monkey *Macaca fascicularis*. J Physiol 427:681–713

Wollmuth LP (1994) Mechanism of Ba^{2+} block of M-like K channels of rod photoreceptors of tiger salamanders. J Gen Physiol 103:45–66. doi:10.1085/jgp.103.1.45